Relative depths of the subsurface peaks of phytoplankton abundance conserved over ocean provinces

Mitsuhide Sato*[1]

satom@nagasaki-u.ac.jp

Takuhei Shiozaki[2]

shiozaki@g.ecc.u-tokyo.ac.jp

Fuminori Hashihama[3]

f-hashi@kaiyodai.ac.jp

Taketoshi Kodama[4]

takekodama@g.ecc.u-tokyo.ac.jp

Hiroshi Ogawa[2]

hogawa@aori.u-tokyo.ac.jp

Hiroaki Saito[2]

hsaito@g.ecc.u-tokyo.ac.jp

Atsushi Tsuda[2]

tsuda@aori.u-tokyo.ac.jp

Shigenobu Takeda[1]

s-takeda@nagasaki-u.ac.jp

Ken Furuya[5]

furuya@fs.a.u-tokyo.ac.jp

[1] Graduate School of Fisheries and Environmental Sciences, Nagasaki University, Nagasaki-shi, Nagasaki, Japan

[2] Atmospheric and Ocean Research Institute, the University of Tokyo, Kashiwa-shi, Chiba, Japan

[3] Tokyo University of Marine Science and Technology, Minato-ku, Tokyo, Japan

[4] Yokohama Field Station, Fisheries Resources Institute, Japan Fisheries Research and Education Agency, Yokohama-shi, Kanagawa, Japan

[5] Graduate School of Science and Engineering, Soka University, Hachioji-shi, Tokyo, Japan

*Corresponding author: Mitsuhide Sato

Running head: Subsurface peak depths of phytoplankton

Keywords: subsurface chlorophyll maximum, *Synechococcus*, *Prochlorococcus*, light, nutrients, flow cytometry

Abstract

Flow cytometric data collected from more than 250 stations in the Pacific and Indian Oceans were analyzed to determine the factors affecting the depth and magnitude of the subsurface abundance maximum of *Synechococcus*, *Prochlorococcus*, and small eukaryotes (< 6 μm). The peak depth of each phytoplankton population estimated by curve fitting was strongly correlated with the depth of the subsurface chlorophyll maximum (SCM). The slope of the regression line demonstrated that the peak depths of *Synechococcus*, *Prochlorococcus*, and small eukaryotes were 74 ± 1%, 88 ± 1%, and 104 ± 1% of the SCM depth (with confidence interval of 95%), respectively. This trend was largely conserved across the different ocean provinces of the Pacific and Indian Oceans. The peaks of *Synechococcus* frequently appeared in the nitrate-depleted layer of subtropical waters, suggesting their high affinity for regenerated and/or organic nutrients. The estimated daily irradiance received at the peak depths of *Synechococcus* and *Prochlorococcus* did not show a distinct latitudinal trend and fluctuated among neighboring stations, whereas that of small eukaryotes slightly increased toward the subarctic region. The present results show that the peak depths of *Synechococcus*, *Prochlorococcus*, and small eukaryotes relative to SCM were globally conserved on average, which is largely in line with the difference in their ability to acquire light and nutrients. However, the absolute light level and nutrient concentrations at the peak depths varied dramatically among neighboring stations, likely affected by physical movements.

Introduction

Oceanic primary production is estimated to contribute to approximately half of the global primary production (Field et al. 1998), which makes marine phytoplankton an essential component of climate control. In addition to numerous elaborate measurements of primary production on research vessels, optical studies using satellite imagery have contributed to progress in the estimation of global phytoplankton biomass and primary productivity (Behrenfeld et al. 2006). Optical measurements using satellites integrate dispersed data collected from research vessels using their high spatial and temporal coverage and resolution.

However, satellites can only obtain information about the sea surface. This is critical, particularly in open ocean areas, where phytoplankton biomass is not constant within the water column. In the stratified water of the open ocean, phytoplankton biomass (based on carbon or chlorophyll) or cell concentration frequently shows a subsurface peak around the bottom of the euphotic zone (Lorenzen, 1966; Saijo et al. 1969; Lande et al. 1989). The occurrence of the subsurface maximum makes it difficult to estimate the areal phytoplankton biomass or productivity from that at the sea surface (Arrigo et al. 2011; Ardyna et al. 2013). To overcome this problem, empirical models have been proposed to estimate the vertical profile of phytoplankton biomass from surface values (Lewis et al. 1983; Morel et al. 1989). The depth and magnitude of the subsurface maximum phytoplankton biomass are indispensable parameters for global mapping of phytoplankton biomass and productivity.

73 The subsurface maximum phytoplankton biomass or chlorophyll concentration is a long-
74 debated issue in biological oceanography, particularly concerning the mechanism of its
75 formation and maintenance (Cullen, 2015). In addition to time-series surveys at fixed
76 stations, measurements using submersible buoys have accumulated a dataset of vertical
77 profiles of chlorophyll concentration and plankton biomass (Cornec et al. 2021a, b), which
78 has made it possible to evaluate the validity of the outputs of biophysical models at a global
79 scale. Modeling studies have suggested that subsurface maxima occur between the light
80 critical depth and nutrient critical depth (Beckman and Hense, 2007; Gong et al. 2015) in
81 equilibrium, as proposed in earlier field studies (Takahashi et al. 1985; Letelier et al. 2004).
82 Photoacclimation, in which phytoplankton cells accumulate more pigment content in dark
83 environments, can contribute to the formation of subsurface chlorophyll maxima (Letelier et
84 al. 2004; Mignot et al. 2014), which sometimes results in subsurface chlorophyll maxima
85 without any associated peak in carbon biomass.
86 Although previous studies have revealed the characteristics of the subsurface maximum of
87 phytoplankton biomass in the open ocean and elucidated the mechanism of its formation and
88 maintenance, many of these studies have treated phytoplankton as a single component,
89 paying little attention to the physiological differences among phytoplankton populations.
90 Field observations have demonstrated that different phytoplankton groups show different
91 vertical distributions (Venrick, 1999; Veldhuis and Kraay, 2004), resulting in vertical

92 segregation of their habitats. When considering the total productivity of the entire community
93 alone, the differences between phytoplankton populations may be trivial. However, if we are
94 to elucidate the biogeochemical cycling and fate of biogenic materials in the food web, the
95 phytoplankton community composition is indispensable information, since the nutritional
96 physiology of phytoplankton and predator–prey relationships differ according to the species
97 or ecotypes of phytoplankton (e.g., diazotrophs and mixotrophs).
98 Additionally, field studies on the subsurface maximum of phytoplankton have been
99 conducted at fixed stations or within a limited area. Whether there is a universal rule or factor
100 that determines the position or magnitude of phytoplankton subsurface maxima throughout
101 the global ocean remains unknown. Considering the geographical variation in the
102 composition of the phytoplankton community, it may be reasonable to assume that the
103 response of phytoplankton biomass to environmental factors varies from one area to another.
104 However, the number of studies comparing subsurface maximum of phytoplankton biomass
105 among different ocean provinces is insufficient to draw conclusions.
106 In the present study, we compared the subsurface maxima of different phytoplankton
107 populations (*Synechococcus*, *Prochlorococcus*, and eukaryotes) in different provinces of the
108 Pacific and Indian Oceans. Flow cytometric data collected from 20 cruises were compiled to
109 create a dataset. The peak depth and magnitude of the three phytoplankton populations were
110 estimated by fitting the sum of sigmoid and Gaussian functions to their discrete vertical

111 profiles. By analyzing them in combination with optical, chemical, and physical data, we
112 aimed to test the validity of the outcome of modeling studies, in which light and nutrient
113 availability determines the depth of phytoplankton biomass peak, and clarify factors that
114 control the depths of subsurface maximum of different phytoplankton populations over
115 different ocean provinces.
116
117 **Materials and Methods**
118 *Profiles of pico- and nanophytoplankton*
119 Flow cytometric data were collected from cruises in the Pacific and Indian Oceans and its
120 marginal seas (Fig. 1 and Table 1). All surveys, except one cruise, were conducted in
121 stratified areas, most of which were carried out between the local spring and fall. Vertical
122 profiles of pico- and nanophytoplankton were obtained from over ten discrete depths using
123 Niskin or Niskin-X samplers. The samples were analyzed onboard without chemical fixation,
124 except for the cruises of R/V Wakataka-maru and Mirai, at which the samples were
125 chemically fixed with glutaraldehyde and frozen in liquid nitrogen (Sato et al. 2006).
126 Samples from 2003 to 2010 were analyzed using a PAS III flow cytometer, and those from
127 2011 to 2018 were analyzed using a CyFlow (Partec). The details of the onboard flow
128 cytometric analyses are described elsewhere (Sato et al. 2010, 2017).
129 Pico- and nanophytoplankton were counted after classifying them as *Prochlorococcus*,

130 *Synechococcus*, nano-sized cyanobacteria, cryptophytes, and other eukaryotes (Sato et al.
131 2010). Although eukaryotes enumerated by flow cytometry include algae of different taxa
132 (Vaulot et al. 2008), and sometimes form multiple distinct clusters on a cytogram, particularly
133 in the subarctic and marginal waters (86 of 257 stations), they were enumerated as a single
134 population in the present study to ensure sufficient cell counts for curve fitting and to grasp
135 the general trend of small eukaryotes as a whole. The maximum nominal cellular diameter of
136 eukaryotes enumerated in the present study was approximately 6 μm, as estimated from a
137 comparison with standard fluorescent beads. This means that larger diatoms or
138 dinoflagellates, which may comprise a significant portion of the phytoplankton biomass in
139 the subpolar or marginal provinces, were excluded from the present analysis. For
140 simplification, we use the term "eukaryotes" to express the pico- and small
141 nanophytoplankton (< 6 μm) measured by flow cytometry in the present study.
142 In the present study, side scatter (SSC) intensity was not used as an index of cellular
143 biomass (see Supporting Information). The product of the mean red fluorescence (FL3) and
144 cell concentration was calculated to estimate the relative contributions of phytoplankton
145 populations to chlorophyll biomass, as applied in previous studies (Zettler et al. 1996, Sato et
146 al. 2009). Cytometric data were obtained using FloMax software (Partec) and gated on FCS
147 Express Flow 6 software (De Novo Software) for enumeration. It should be noted that
148 *Prochlorococcus* in surface water (HL-type *Prochlorococcus*) is likely to be underestimated

149 because of its faint chlorophyll fluorescence. Although this may lead to an overestimation of
150 the relative magnitude of the subsurface maximum, the position (depth) of their peak is only
151 slightly affected.
152 Measurements of environmental parameters (temperature, salinity, chlorophyll a
153 fluorescence, light intensity, and nutrient concentrations) are detailed in Supporting
154 Information.
155
156
157
158 *Mathematical and statistical procedures*
159 To characterize the vertical distribution pattern of pico- and nanophytoplankton cell
160 concentrations, a mathematical function was fitted to the relationship between depth and cell
161 concentration, and the parameters that represent the position of the subsurface maximum
162 layer and its relative magnitude were extracted.
163 The typical vertical distribution patterns of pico- and nanophytoplankton in stratified open
164 water showed three characteristics: (1) subsurface peaks, (2) relatively constant
165 concentrations above the peak, and (3) sharp declines below the peak. To reproduce such a
166 typical vertical distribution, we adopted the sum of a normal distribution function and logistic
167 function expressed as

$$y = Me^{-\frac{(x-p)^2}{a}} + C\frac{1}{1+e^{b(x-p)}} \quad (1)$$

Here, x and y denote the depth and cell concentration, respectively, and five constants a, b, p, C, and M were optimized for each vertical distribution by curve fitting. In the present study, the peak of the normal distribution and the flexion point of the logistic curve were assumed to occur at the same point, p, to reduce the calculation amount. We selected these functions to simplify the calculation and more readily interpret the outcome of the estimated constants. A normal distribution around the subsurface maximum of phytoplankton biomass in subtropical waters successfully reproduced the real vertical distribution (Gong et al. 2015), and Equation (1) can be optimally fitted to most of the vertical distribution patterns of pico- and nanophytoplankton in the open ocean with a relatively small amount of calculation (Fig. 2).

From the five constants in Equation (1), that is, a, b, p, C, and M, the parameters that characterize the vertical distribution pattern can be readily derived. In this formula, the cell concentration at depth p can be calculated as ($M + C/2$), where C represents the ideal cell concentration at negative infinity. The M/C ratio can be used to index the relative peak strength compared with the surface cell concentration. As mentioned above, p represents the peak depth, and a is an index of the width of the peak. Parameter b is an attenuation index in the logistic function.

Curve fitting was performed using software OriginPro 2015 (OriginLab). Levenberg–

187 Marquardt's method was applied for the repetition algorithm. All parameters were confined
188 to a positive value, and the maximum value for p was set to 200 m. When the fitting did not
189 converge successfully, the data at the station were not included in the following analysis. All
190 other fitting, regression, or statistical analyses were performed using OriginPro, R (version
191 4.1.1) or Microsoft Excel. The spatial autocorrelation of the environmental parameters was
192 tested based on Moran's I values calculated using the *ape* library of R. The study area was
193 partitioned into ocean provinces according to Longhurst (2007).
194
195 **Results**
196 Of the 257 stations surveyed during 20 cruises (Table 1), 231, 160, 17, 28, and 240
197 profiles were successfully fitted to Equation (1) (see Materials and Methods) for
198 *Synechococcus*, *Prochlorococcus*, nano-sized cyanobacteria, cryptophytes, and other
199 eukaryotes, respectively. At the other stations, the fitting failed because the phytoplankton
200 population was absent or their vertical profile did not show a distinctive subsurface peak.
201 Further analyses of nano-sized cyanobacteria and cryptophytes were not performed in the
202 present study because their sample size was small due to their limited occurrence, and their
203 subsurface peak was indistinctive ($M/C < 0.5$) at most of the stations. During the MR10-01
204 cruise (Table 1), the high-latitudinal area in Kuroshio Province was surveyed during the
205 winter season, when strong mixing occurred. During this cruise, the fitting failed in most

206 cases, and the *M/C* value was almost zero. The entire dataset presented in this study is listed
207 in Table S1.
208 The horizontal trend in the peak depth of cell concentration was similar for the three
209 populations of pico- and nanophytoplankton, *Synechococcus*, *Prochlorococcus*, and
210 eukaryotes (Fig. S2). The peak depth was deeper in the subtropical gyres than in the subarctic
211 waters, equatorial areas, East China Sea, and Bay of Bengal. Among the three subtropical
212 gyres surveyed in the present study (two in the Pacific Ocean and one in the Indian Ocean),
213 the South Pacific subtropical gyre showed the deepest peak depth of all three populations.
214 Although the longitudinal variation in the peak depths in the subtropical Pacific was not as
215 evident as the latitudinal variation, the peak seemed deeper towards the east in the North
216 Pacific subtropical areas, especially in eukaryotes. Although the longitudinal trend in the
217 South Pacific subtropical gyre was not clear owing to the small sample size, the peak depth at
218 170 °W seems shallower compared with that in the eastern area.
219 Compared with the peak depths, the relative magnitudes of the subsurface peaks of the
220 cell concentration (*M*/*C* ratio) showed a less clear horizontal trend (Fig. S2). As a general
221 trend, the *M*/*C* ratio was smaller than 1 in the high-latitude areas, indicating that the
222 subsurface abundance peak was unclear in these areas. This may reflect the low contribution
223 of carbon biomass accumulation to the subsurface chlorophyll maximum at high latitude
224 (Cornec et al. 2021; Masuda et al. 2021). The *M*/*C* ratio was highly variable between

neighboring stations, which made its horizontal trend even more unclear.

The peak depths of the three pico- and nanophytoplankton populations were compared with the mixed layer, SCM, and nitracline depths on a regional basis (Fig. 3). The peak depths were highly correlated with one another and SCM depths, which were deeper in the subtropical provinces, including the western area of the North Pacific Subtropical Front (NPSTW), the eastern and western areas of the North Pacific Tropical Gyre (NPTGE and NPTGW, respectively), and the South Pacific Subtropical Gyre (SPSG), than in the other areas. In contrast, the mixed layer depth showed a much smaller interprovincial variation, in which it was slightly deeper in the Indian monsoon gyre province (MONS) and the NPTGE and NPTGW (Fig. 3D). The longitudinal difference in the peak depth was not statistically different between NPTGE and NPTGW for any of the three populations (Tukey-Kramer test, $p > 0.05$). The nitracline depth showed an interprovincial variation, which is similar to that of SCM (Fig. 3F).

The peak depths of *Synechococcus*, *Prochlorococcus*, and eukaryote cell concentrations were highly positively correlated with SCM depth, when all the data from 19 ocean provinces were compiled (Fig. 4). A positive correlation was also observed for each ocean province, including marginal seas or subarctic provinces. Moreover, it seems that data from all ocean provinces are distributed around the same straight line, except for some stations in the Pacific Subarctic Gyre (PSAG), where peak depths seemed to deviate above the line. Three simple

linear relationships were derived as follows (coefficients are shown with standard errors):

$$Synechococcus: Peak\ \ depth = (0.47\ \ \pm 0.02) \times SCM + (25.2\ \ \pm 2.2)\quad (R^2 = 0.64)$$

$$Prochlorococcus:\ \ Peak\ \ depth = (0.72\ \ \pm 0.04) \times SCM + (16.6\ \ \pm 3.5)\quad (R^2 = 0.72)$$

$$Eukaryotes: Peak\ \ depth = (0.95\ \ \pm 0.03) \times SCM + (9.1\ \ \pm 2.4)\quad (R^2 = 0.85)$$

When the intercept was fixed to 0, the regression was again highly significant:

$$Synechococcus: Peak\ \ depth = (0.74\ \ \pm 0.01) \times SCM\quad (R^2 = 0.94)$$

$$Prochlorococcus:\ \ Peak\ \ depth = (0.88\ \ \pm 0.01) \times SCM\quad (R^2 = 0.96)$$

$$Eukaryotes: Peak\ \ depth = (1.04\ \ \pm 0.01) \times SCM\quad (R^2 = 0.97)$$

The slope of the regression line was in the order of *Synechococcus*, *Prochlorococcus*, and eukaryotes, indicating an inter-regional trend in the open ocean, where the peak of *Synechococcus* cell concentration occurred at the shallowest depth of the three, while eukaryotes showed the deepest peak. In the range of SCM < 40 m, which included profiles from the subpolar and marginal provinces, the deviation from the regression line was larger. At these stations, chlorophyll fluorescence and phytoplankton abundance did not always show a clear peak. When these profiles were excluded from the dataset, the correlation became stronger and the intercept of the regression line became smaller (19.3 ± 4.0, 5.2 ± 4.3, and −5.1 ± 3.8 for *Synechococcus*, *Prochlorococcus*, and eukaryotes, respectively). Compared with the SCM depth, the mixed layer depth showed a much weaker correlation with the peak depth of any of the phytoplankton groups examined (Fig. S3). The coefficients

of determination (R^2) for *Synechococcus*, *Prochlorococcus*, and eukaryotes were 0.20, 0.01, and 0.04, respectively, whereas the slope of the regression line was significantly different from zero ($p < 0.05$) only for *Synechococcus* and eukaryotes. When analyzed for each ocean province, the correlation became much weaker ($p > 0.05$). The correlation was only significant in certain subtropical and tropical provinces, and the slope and intercept of the regression line differed among different provinces.

The potential density anomaly (σ_θ) at the peak depths of the three phytoplankton groups calculated using the pressure, temperature, and salinity obtained from the CTD sensor showed a U-shaped latitudinal distribution with a minimum value around the equator (Fig. S4). The variation at similar latitudes within a specific ocean province was relatively small, except in the Kuroshio and East China Sea provinces, where the intrusion of less saline coastal water greatly affected the density structure of the water column. The σ_θ values showed strong spatial autocorrelation, and the *p*-values based on Moran's *I* were $< 10^{-15}$ for all three phytoplankton groups. As speculated from the peak depths of the three phytoplankton groups (Figs. 3 and 4), the σ_θ values at the peaks of eukaryotes were generally greater than those of the other two groups, and their latitudinal variation was the smallest among the three groups (Fig. S4).

The latitudinal variation in the mean PAR at the peak depth was smaller than the variation among the neighboring stations (Fig. 5). The mean PAR at the peak depth of *Synechococcus*

282 ranged between 0.2 and 9 mol quanta m^{-2} d^{-1}, averaging 2.2 ± 1.7 (mean ± standard
283 deviation) mol quanta m^{-2} d^{-1}(Fig. 7A), but no apparent geographical trend was observed. As
284 for *Synechococcus*, *Prochlorococcus* did not exhibit any geographical trend (Fig. 5B), and the
285 mean PAR at their peak depth was 1.2 ± 1.2 mol quanta m^{-2} d^{-1}. The latitudinal variation was
286 marginally distinguishable in the mean PAR at the peak depth of eukaryotes (Fig. 5C), which
287 was significantly higher (Kruskal-Wallice test, $p < 0.01$) in the subarctic provinces (2.6 ± 1.5
288 mol quanta m^{-2} d^{-1}) than in the other areas (1.0 ± 1.9 mol quanta m^{-2} d^{-1}). In both the
289 Kuroshio and North Pacific Subtropical Front (NPST) provinces in the transition area from
290 the subtropical to the subarctic regions, the PAR irradiance showed a significant positive
291 correlation with latitude ($p < 0.01$). In relation to this, the PAR irradiance in the North Pacific
292 Subtropical Gyre (NPSG) (0.3 ± 0.4 mol quanta m^{-2} d^{-1}) was significantly lower ($p < 0.001$)
293 than in the other areas. The mean PAR irradiance at the peak depth of eukaryotic
294 phytoplankton was lower in the SPSG than at similar latitudes in the Indian Ocean (Kruskal-
295 Wallis test, $p < 0.01$), reflecting their deeper peak in the South Pacific (Fig. 5C). The *p*-values
296 of spatial autocorrelation of the mean PAR at the peak depth were larger than those of σ_θ,
297 0.01, 0.05, and 0.13 for *Synechococcus*, *Prochlorococcus*, and eukaryotes, respectively.
298 The estimated N+N concentrations at the peak depths of each phytoplankton group (Figs.
299 6 and S5) were more dispersed than PAR irradiance and showed a clearer latitudinal
300 variation, especially for *Synechococcus* (Fig. 6A). The N+N concentration at the peak depth

301 of *Synechococcus* was frequently below the detection limit of the conventional method (50
302 nM) in subtropical gyres (Figs. 6A and S5A). The proportion of data points where the N+N
303 concentration at the abundance peak of *Synechococcus* was below the detection limit was
304 91% (29 of 32) and 64% (9 of 14) in the North Pacific Tropical Gyre (NPTG) and the SPSG,
305 respectively. In contrast, in the subarctic areas, the N+N concentration at the peak depth of
306 *Synechococcus* was higher than 10 μM. In contrast, most of the eukaryote peaks were located
307 on or below the nitracline (Fig. 3F), and N+N concentrations at their peak depths were rarely
308 below the detection limit (Figs. 6C and S5C). *Prochlorococcus* showed an intermediate trend
309 between *Synechococcus* and eukaryotes (Fig. 6B), and the variation within an ocean province
310 was large, particularly in the subtropical and tropical gyres (Fig. S5B). For *Prochlorococcus*,
311 the proportion of data points where the N+N concentration was below the detection limit was
312 66% (21 of 32) and 63% (10 of 16) in the NPPTG and SPTG, respectively. The large
313 variation within an ocean province seemingly reflects the fact that the peak depth of
314 *Prochlorococcus* is frequently located near the nitracline, where the N+N concentration
315 varies most dramatically vertically. The spatial autocorrelation of the N+N concentration was
316 significant but weaker than that of σ_θ, with p-values $< 10^{-5}$.
317 The relative magnitude of the subsurface peak, *M/C*, was not significantly correlated with
318 any of the latitudes, daily mean PAR, or N+N concentration at the peak depth ($p > 0.05$) for
319 all three phytoplankton groups. In the generalized linear model with a gamma distribution,

320 the slope was not significantly different from zero ($p > 0.05$) regardless of the link function
321 adopted.
322
323 **Discussion**
324 *Global trends of phytoplankton subsurface peak depths*
325 The present study clearly demonstrated that the peak depths of the pico- and
326 nanophytoplankton cell concentrations varied horizontally with respect to the depth of the
327 SCM (Figs. S2 and 4). The latitudinal variation was much greater than the longitudinal
328 variation and the peak depth was deeper within the tropical and subtropical gyres in both
329 hemispheres (Fig. 3). Although data obtained by automated floats suggest that a significant
330 proportion of SCM in subtropical gyres is formed by photoacclimation and is not
331 accompanied by a peak in particulate organic carbon (Cornec et al. 2021a), the present study
332 showed that the peaks in phytoplankton cell concentrations were observed even in these
333 areas. Although it is worth noting that the peaks of cell abundance were not always
334 concomitant with those of the population biomass, the present results (Fig. S1) demonstrate
335 that it is valid to use the peak depth of phytoplankton cell concentration as a proxy for
336 biomass peak depth (see Supporting Information).
337 The peak depths of *Synechococcus*, *Prochlorococcus*, and eukaryotes, were highly
338 hierarchized vertically, particularly in the range of SCM > 40 m. The peak of *Synechococcus*

was the shallowest, whereas that of eukaryotes was the deepest, with the peak of *Prochlorococcus* occurring between them. This trend was seen in stratified waters within the Pacific and Indian Oceans, including the subarctic and marginal regions (Fig. 4). In less stratified waters, for example, the Kuroshio province in the winter season, subsurface peaks of cell concentrations were not detected. In the following paragraphs, we discuss the present results in relation to previous model studies and laboratory culture studies to elucidate the factors that can account for the vertical distribution pattern of each phytoplankton population.

Previous biophysical model studies have suggested that the subsurface maximum of phytoplankton biomass in stratified open water occurs between the nutrient compensation depth over the nutricline and light compensation depth (Beckman and Hense 2007; Gong et al. 2015). This can account for the deeper peak depth in subtropical and tropical gyres, where strong surface PAR and low light extinction allow light penetration into the deep layer. The mean daily PAR values at SCM have been reported from the subtropical areas including the North Pacific (0.5 mol quanta m^{-2} d^{-1}, Letelier et al. 2004), the South Pacific (~0.08 mol quanta m^{-2} d^{-1}, Xing et al. 2013), and the North Atlantic (0.07 mol quanta m^{-2} d^{-1}, Cornec et al. 2021a), showing a large study-to-study variation, which is consistent with the large variation in the PAR values at abundance peak within a small area (Fig. 5). These values were within the range of the mean daily PAR at the peak of eukaryotes in the NPSG in the present study (0.3 ± 0.4 mol quanta m^{-2} d^{-1}), which is reasonable considering the nearly 1:1

358 relationship between the eukaryote peak and SCM depths (Fig. 4C). However, the PAR level
359 at the SCM in the Black Sea was found to have fluctuated in a higher range (0.15–3.00 mol
360 quanta m^{-2} d^{-1}, Kubryakov et al. 2020). The higher PAR at the SCM in midlatitude areas than
361 in subtropical areas was recently observed from global observations as well (Yasunaka et al.
362 2022), which is consistent with the increase in the PAR level at the peak depth of eukaryotes
363 toward higher latitude in the northern hemisphere in the present study.
364 One of the most important findings of the present study was that the relative depth of
365 *Synechococcus*, *Prochlorococcus*, and eukaryotes to the SCM depth was relatively constant
366 across the different ocean provinces studied (Fig. 4), except for some stations in the subpolar
367 and marginal provinces, where SCM was not distinctly formed. This is surprising considering
368 that the taxonomic composition of eukaryotic phytoplankton in subsurface waters is different
369 among the ocean provinces (Furuya, 1990; Suzuki et al. 2002). Additionally, pico-sized
370 cyanobacteria, *Synechococcus* and *Prochlorococcus*, show distinct geographic variations in
371 their composition of different ecotypes (Zwirglmaier et al. 2007; 2008), which possess
372 different physiological and nutritional properties.
373 It is widely known that the cellular pigment content of phytoplankton increases with depth
374 because of photoacclimation and/or photoadaptation (Latasa et al. 2017). Thus, the
375 subsurface peak of the total pigment content of each phytoplankton group is expected to be
376 located deeper than the phytoplankton cell abundance maximum. Taking this effect into

account, the contribution of *Prochlorococcus*, the peak of which was located approximately 12% shallower than that of SCM (Fig. 4B) on average, is likely to be an important component of SCM, especially in subtropical regions. The finding that the relationship between the peak depth of eukaryotes and SCM depth was close to the 1:1 line (Fig. 4C) suggests that eukaryotes significantly contribute to the chlorophyll content in the SCM layer over different ocean provinces. This is reinforced by the taxon-specific chlorophyll-based biomass estimation of phytoplankton using photosynthetic pigment analyses (Mackey et al. 1998; DiTullio et al. 2003), which found that *Prochlorococcus* and eukaryotic phytoplankton contributed in large proportions to the chlorophyll biomass in the subsurface water. The integrated FL3 intensities of the three phytoplankton groups (Fig. S6) also support the dominance of *Prochlorococcus* and eukaryotes in chlorophyll biomass at the SCM over different ocean provinces, whereas the relative contributions of the two groups varied according to province.

However, the correlation of each phytoplankton subsurface peak depth with SCM was weaker in the range of SCM < 40 m (Fig. 4). In this region, the SCM is often unclear, and the chlorophyll fluorescence is relatively constant over its cline. In areas affected by riverine input, such as the East China Sea, the chlorophyll maximum is sometimes formed near the surface by dinoflagellates or buoyant cyanobacteria (Yue et al. 2021), which are not in the detection range of a flow cytometer (see Materials and Methods). This likely accounts for the

deeper subsurface peaks of the three phytoplankton groups compared with the SCM in this area (Fig. 4). In addition, it is possible that the subsurface peak of cell abundance was formed by sinking cells, which are no longer vital and contain small amounts of pigments. Data profiles obtained by automated floats also show that the subsurface maxima of chlorophyll and particulate organic matter are formed only during a limited period of the year in subpolar areas (Cornec et al. 2021a). Therefore, the conserved relative peak depths of each phytoplankton group found in the present study were applied only to stratified water, where a distinct SCM was maintained.

Vertical hierarchization of phytoplankton populations

In the equilibrium biophysical model (Beckman and Hense 2007; Gong et al. 2015), affinity to nutrients and light harvesting capacity are considered to largely determine the depth at which the maximum biomass of phytoplankton occurs, assuming that grazing and vertical diffusion are constant. Thus, the populations that accumulate at shallow depths demand high PAR irradiance but can survive on trace amounts of regenerated nutrients. In contrast, a population that accumulates in the nutrient-rich deep layer is required to effectively harvest the limited intensity of light. Considering the outcomes of these model studies, the overall trends in the peak depths of the three phytoplankton groups seem to be explained by their different physiological traits for nutrient and light acquisition. In the following paragraphs, we discuss in more detail how these factors affect the relative peak

depth of each phytoplankton group.

In the present study, at the peaks of *Synechococcus*, N+N was depleted to an undetectable level, particularly in the subtropical and tropical gyres (Figs. 6A and S5A). This outcome indicates that *Synechococcus* was most abundant at depths far above the nitracline (Fig. 3F), where the supply of oxidized nitrogen nutrients via upwelling or turbulence was scarce. Since it is unlikely that *Synechococcus* facilitates nitrogen fixation or phagotrophy to fulfill nitrogen demand, regenerated (ammonium) and/or organic nitrogen nutrients including urea (Collier et al. 1999), amino acids (Paerl 1991), and peptides (Martinez and Azam 1993) are assumed to be promising nitrogen sources for *Synechococcus* at their abundance peaks. .

The N+N concentration at which the *Prochlorococcus* cell concentration peaked was generally higher than that of *Synechococcus*, and highly variable among neighboring stations in the subtropical and tropical gyres (Fig. 6B). This suggests that the peaks of *Prochlorococcus* appeared around the nitracline (Fig. 3F), where the vertical gradient of N+N concentration was the largest. Although axenic cultures of *Prochlorococcus* lack the ability to incorporate or assimilate nitrate or nitrite and to depend on ammonium and organic nitrogen compounds as a nitrogen source (Rippka et al. 2000; Moore et al. 2002; Zubkov et al. 2003), recent field studies (Casey et al. 2007; Berthelot et al. 2019) and genomic analyses (Martiny et al. 2009; Barube et al. 2015) have demonstrated that some strains of *Prochlorococcus* can assimilate nitrate and nitrite, and that assimilation occurs particularly in subsurface water,

434 whereas those that cannot utilize nitrate or nitrite mainly occupy the sunlit surface water. The
435 ability of *Prochlorococcus* to assimilate various chemical forms of nitrogen compounds
436 likely enables it to remain highly abundant in environments with a wide range of N+N
437 availability, as observed in the present study (Fig. 6B).
438 If we assume that the vertical segregation of different phytoplankton groups is determined
439 only by nutrient acquisition traits, the shallower peaks of *Synechococcus* than those of
440 *Prochlorococcus* cannot be explained. The smaller cell diameter of *Prochlorococcus* is
441 advantageous for incorporating a lower concentration of regenerated nutrients, which can
442 make them more prosperous in shallower waters than *Synechococcus*, contrary to the trend
443 observed in the present study (Figs. 3 and 4). A previous field experiment in the North Pacific
444 demonstrated that the proportion of regenerated nitrogen in the total assimilated nitrogen was
445 similarly high for both *Synechococcus* and *Prochlorococcus* (Berthelot et al. 2019), which
446 supports the idea that both cyanobacteria depend on regenerated nitrogen to similar degrees.
447 This suggests that their potential to incorporate regenerated nutrients at an extremely low
448 level is not sufficient to explain the shallower peak of *Synechococcus* than that of
449 *Prochlorococcus*. Another factor that can account for this difference may be the
450 characteristics of light utilization.
451 The different absorption spectra of photosynthetic pigments in *Synechococcus* and
452 *Prochlorococcus* can explain the shallower peak in *Synechococcus*. This concept was

453 incorporated into the biophysical model of Hickman et al. (2010), which successfully
454 reproduced the vertical segregation of *Synechococcus* and *Prochlorococcus*. While
455 *Synechococcus* can absorb green light using phycoerythrin, other phytoplankton groups that
456 inhabit deeper water utilize different wavelength regions of PAR for photosynthesis, which
457 were not utilized by *Synechococcus*. The high diversity of photosynthetic pigment repertoires
458 in eukaryotes may reflect niche segregation via light physiology. Niche segregation of
459 different phytoplankton groups based on the spectra of photosynthetic pigments has been
460 proposed for the horizontal distribution of phytoplankton worldwide as well (Holtrop et al.
461 2021). The results of this study provide further support for the applicability of the biophysical
462 model to a wide area of the open ocean.

463 The lack of a significant latitudinal trend in the mean daily PAR irradiance received at the
464 subsurface maxima of *Synechococcus* and *Prochlorococcus* in stratified waters (Figs. 5A and
465 B) in contrast to the large variation among neighboring stations suggests that the
466 geographical variation in their light physiology is not sufficiently large to cause a detectable
467 change in their critical light depth, assuming that the maximum layer occurs above their light
468 critical depth. Thus, the geographical segregation of different ecotypes of *Synechococcus* and
469 *Prochlorococcus* (Zwirglmaier et al. 2007; 2008), which possess different nutritional and
470 light physiology, does not strongly affect the population compensation light intensity of these
471 pico-sized cyanobacteria in the subsurface water and the latitudinal trend of their peak depth.

In contrast to cyanobacteria, eukaryotes showed weak latitudinal variation in PAR irradiance received at their subsurface maximum (Fig. 5C). This is likely due to the phylum-to-class-level geographical variation in the composition of eukaryotic phytoplankton (Furuya, 1990; Suzuki et al. 2002). Algae of different phyla or classes possess different repertoires of photosynthetic and accessory pigments, resulting in different absorption spectra. Recently, a global dataset demonstrated that the daily PAR level at SCM varies latitudinally, which is lower than the photosynthetically active level (0.415 mol quanta m^{-2} d^{-1}) in subtropical waters but higher in equatorial and mid-latitude areas (Yasunaka et al. 2022). This latitudinal variation is consistent with the present observations that chlorophyll biomass is dominated by eukaryotes and *Synechococcus* at middle to high latitudes (Fig. S6) and that the mean PAR level at the peak of eukaryotes was slightly elevated toward higher latitudes in the Northern Hemisphere (Fig. 5C), suggesting that inter-regional variations in the phytoplankton community structure and/or physiology can be associated with light intensity at the SCM.

Future directions

The strong positive correlation among each subsurface maximum depth when the entire dataset from different ocean provinces was analyzed together (Fig. 4) demonstrates that there is a widely observed trend for the relative depth of each phytoplankton population in the stratified waters of the Pacific and Indian Oceans. Since a shallower subsurface peak of

491 *Synechococcus* than that of *Prochlorococcus* and eukaryotes was observed for the subtropical
492 Atlantic (Durand et al. 2001) as well, this trend is possibly a global one. On the other hand,
493 the observation that the depth and magnitude of the abundance peak varied considerably
494 among overlapping or neighboring stations (Figs. S2 and 4) suggests that each data point was
495 not in the equilibrium state proposed by modeling studies.

496 One factor that may account for the variability in the peak depth and magnitude is the
497 diurnal change in the mixed layer depth (Salihoglu 2009), oscillation by the internal wave
498 (Cullen et al. 1983), and mesoscale eddies (Li and Hansell, 2016; Cornec et al. 2021b). The
499 strong spatial autocorrelation in the σ_θ values at the peak depths (Fig. S4) demonstrates that
500 the density at the subsurface peak was highly similar among the neighboring stations, as
501 compared to the PAR level or N+N concentrations, suggesting that the subsurface abundance
502 peak moves vertically on the isopycnic surface. In addition to the physical uplift of the
503 subsurface peak itself, decoupling of the light depth and nutricline can affect the depth and
504 magnitude of the peak (Li and Hansell 2016; Xiu and Chai 2020). Although using a large
505 dataset (Fig. 4) can make the overall general trend visible, the vertical depth averaged over
506 different time points or longitudes on the fixed depth axis can obscure the peak of
507 phytoplankton biomass (Hense and Beckmann, 2008; Buitenhuis et al. 2012). Non-
508 equilibrium biophysical models incorporating time parameters are required to reproduce the
509 subsurface maximum in a real environment, even in highly stratified subtropical waters

510 during the summer.

511 In addition to the factors described above, many physiological and ecological factors may
512 also affect the vertical distribution of phytoplankton. In previous biophysical models,
513 nutritional strategies other than obligate autotrophy based on nitrate, nitrite, and ammonium,
514 have rarely been assumed. Although phagotrophy is a strategy for pico- and nano-sized
515 phytoplankton to overcome deficiencies in major nutrients (Arenovski et al. 1995; Sato et al.
516 2017), the contribution of mixotrophs to the total phytoplankton is generally minor or
517 negligible around the SCM in the open ocean (Arenovski et al. 1995; Sato and Hashihama
518 2019). In addition to bottom-up regulation, top-down regulation by microzooplankton grazing
519 may also affect the vertical distribution of phytoplankton. Microzooplankton grazing
520 demonstrates diel variation (Ng and Liu 2016), which can partly account for the temporal
521 change in the position or magnitude of the subsurface maxima of phytoplankton. However,
522 microzooplankton and phytoplankton abundance affect each other, which makes modeling
523 microzooplankton vertical distributions more complex (Li et al. 2011). A large dataset of
524 microzooplankton abundance and grazing is required at comparably high temporal and spatial
525 resolutions to reveal the interaction between phytoplankton and microzooplankton. The
526 inclusion of these parameters may explain the drastic variation in the relative magnitude of
527 the subsurface peak (*M/C*), which was not explained by the environmental parameters
528 measured in this study.

Conclusion

The present study demonstrated that the relative depths of peak abundance of *Synechococcus*, *Prochlorococcus*, and eukaryotes to that of SCM were highly conserved throughout the Pacific and Indian Oceans, and that the depth patterns of their subsurface peaks were in accordance with the physiological traits of their light and nutrient utilization reported in previous studies. These findings on the general trend of the peak depths of different phytoplankton groups make it possible to estimate the average pattern of the vertical distribution of each phytoplankton group in relation to that of chlorophyll. On the other hand, relatively large variations in the PAR level and nutrient availability at the subsurface peak depth between neighboring stations suggest that the vertical distribution of each phytoplankton group was not in the equilibrium state as predicted from model studies and was likely affected by temporally varying factors, including internal waves or eddies, and/or diel variations in physiological parameters. More elaborate trait-based biophysical models that do not assume equilibrium will help elucidate which factors affect the discrepancy from the vertical distribution of phytoplankton predicted from the equilibrium model.

Supporting information

Table S1. The dataset of peak depths, peak ratios, mixed layer depths, SCM depths, 1% light

548 depths, and σ_θ, daily mean PAR, and N+N concentration at the peak of each phytoplankton
549 group, together with station information.
550 Supplemental methods and Figs. S1-S6 are provided as Supporting Information.
551
552 **Acknowledgements**
553 We greatly appreciate all the crew members of the R/V Hakuho-maru, Tansei-maru, Shinsei-
554 maru, Mirai and Wakataka-maru for their assistance in ship work. Drs. Xin Liu and Iwao
555 Tanita kindly provided the dataset of nutrient concentrations. Dr. Sachihiko Ito provided
556 advice on physical processes. This study was financially supported by JSPS grants
557 (22710006, 24710004, 25850129, 15H02802, 17H01852, and 18H03361) and MEXT grants
558 (18067007, 24121003, and 24121006).
559
560
561 **Conflicts of interest**
562 The authors declare no conflicts of interest directly relevant to the content of this article.
563
564 **References**
565 Ardyna, M. and others 2013. Parameterization of vertical chlorophyll a in the Arctic Ocean:
566 Impact of the subsurface chlorophyll maximum on regional, seasonal, and annual
567 primary production estimates. Biogeosciences 10: 4383-4404.

568 Arenovski, A. L., E. L. Lim, and D. A. Caron. 1995. Mixotrophic nanoplankton in
569 oligotrophic surface waters of the Sargasso Sea may employ phagotrophy to obtain
570 major nutrients. J. Plankton Res. 17: 801-820.
571 Arrigo, K. R., P. A. Matrai, and G. L. van Dijken. 2011. Primary productivity in the Arctic
572 Ocean: Impacts of complex optical properties and subsurface chlorophyll maxima on
573 large-scale estimates. J. Geophys. Res.: Oceans 116.
574 Beckmann, A., and I. Hence. 2007. Beneath the surface: Characteristics of oceanic
575 ecosystems under weak mixing conditions – A theoretical investigation. Prog.
576 Oceanogr. 75: 771-796.
577 Behrenfeld, M. J. and others 2006. Climate-driven trends in contemporary ocean productivity.
578 Nature 444: 752-755.
579 Berthelot, H. and others 2019. NanoSIMS single cell analyses reveal the contrasting nitrogen
580 sources for small phytoplankton. ISME J. 13: 651-662.
581 Berube, P. M. and others 2015. Physiology and evolution of nitrate acquisition in
582 Prochlorococcus. ISME J. 9: 1195-1207.
583 Buitenhuis, E. T. and others 2012. Picophytoplankton biomass distribution in the global
584 ocean. Earth Syst. Sci. Data 4: 37-46.
585 Casey, J. R., M. W. Lomas, J. Mandecki, and D. E. Walker. 2007. *Prochlorococcus*
586 contributes to new production in the Sargasso Sea deep chlorophyll maximum.
587 Geophys. Res. Lett. 34: 5.
588 Collier, J. L., B. Brahamsha, and B. Palenik. 1999. The marine cyanobacterium
589 *Synechococcus* sp. WH7805 requires urease (urea amidohydrolase, EC 3.5.1.5) to
590 utilize urea as a nitrogen source: molecular-genetic and biochemical analysis of the
591 enzyme. Microbiology 145: 447-459.
592 Cornec, M. and others 2021a. Deep chlorophyll maxima in the global ocean: Occurrences,
593 drivers and characteristics. Global Biogeochem. Cy. 35: e2020GB006759.

Cornec, M., R. Laxenaire, S. Speich, and H. Claustre. 2021b. Impact of mesoscale eddies on deep chlorophyll maxima. Geophys. Res. Lett. 48: e2021GL093470.

Cullen, J. J., E. Stewart, E. Renger, R. W. Eppley, and C. D. Winant. 1983. Vertical motion of the thermocline, nitracline and chlorophyll maximum layers in relation to currents on the Southern California Shelf. J. Mar. Res. 41: 239-262.

Cullen, J. J. 2015. Subsurface chlorophyll maximum layers: Enduring enigma or mystery solved? Ann. Rev. Mar. Sci. 7: 207-239.

DiTullio, G. R., M. E. Geesey, D. R. Jones, K. L. Daly, L. Campbell, and W. O. Smith Jr. 2003. Phytoplankton assemblage structure and primary productivity along 170°W in the South Pacific Ocean. Mar. Ecol. Prog. Ser. 255: 55-80.

DuRand, M. D., R. J. Olson, and S. W. Chisholm. 2001. Phytoplankton population dynamics at the Bermuda Atlantic Time-series station in the Sargasso Sea. Deep Sea Res. II 48: 1983-2003.

Field, C. B., M. J. Behrenfeld, J. T. Randerson, and P. Falkowski. 1998. Primary Production of the Biosphere: Integrating Terrestrial and Oceanic Components. Science 281: 237-240.

Furuya, K. 1990. Subsurface chlorophyll maximum in the tropical and subtropical western Pacific Ocean: Vertical profiles of phytoplankton biomass and its relationship with chlorophyll *a* and particulate organic carbon. Mar. Biol. 107: 529-539.

Gong, X., J. Shi, H. W. Gao, and X. H. Yao. 2015. Steady-state solutions for subsurface chlorophyll maximum in stratified water columns with a bell-shaped vertical profile of chlorophyll. Biogeosciences 12: 905-919.

Hense, I., and A. Beckmann. 2008. Revisiting subsurface chlorophyll and phytoplankton distributions. Deep-Sea Res. I 55: 1193-1199.

Hickman, A. E., S. Dutkiewicz, R. G. Williams, and M. J. Follows. 2010. Modelling the effects of chromatic adaptation on phytoplankton community structure in the

620 oligotrophic ocean. Mar. Ecol. Prog. Ser. 406: 1-17.
621 Kubryakov, A. A., A. S. Mikaelyan, S. V. Stanichny, and E. A. Kubryakova. 2020. Seasonal
622 stages of chlorophyll-*a* vertical distribution and its relation to the light conditions in
623 the Black Sea from Bio-Argo measurements. J. Geophys. Res.: Oceans 125, doi:
624 10.1029/2020JC016790.
625 Lande, R., W. K. W. Li, E. P. W. Horne, and A. M. Wood. 1989. Phytoplankton growth rates
626 estimated from depth profiles of cell concentration and turbulent diffusion. Deep Sea
627 Res. A 36: 1141-1159.
628 Latasa, M., A. M. Cabello, X. A. G. Morán, R. Massana, and R. Scharek. 2017. Distribution
629 of phytoplankton groups within the deep chlorophyll maximum. Limnol. Oceanogr.
630 62: 665-685.
631 Letelier, R. M., D. M. Karl, M. R. Abbott, and R. R. Bidigare. 2004. Light driven seasonal
632 patterns of chlorophyll and nitrate in the lower euphotic zone of the North Pacific
633 Subtropical Gyre. Limnol. Oceanogr. 49: 508-519.
634 Lewis, M. R., J. J. Cullen, and T. Platt. 1983. Phytoplankton and thermal structure in the
635 upper ocean: consequences of nonuniformity in chlorophyll profile. J. Geophys. Res.
636 88: 2565-2570.
637 Li, Q. P., P. J. S. Franks, and M. R. Landry. 2011. Microzooplankton grazing dynamics:
638 -parameterizing grazing models with dilution experiment data from the California
639 Current Ecosystem. Mar. Ecol. Prog. Ser. 438: 59-69.
640 Li, Q. P., and D. A. Hansell. 2016. Mechanisms controlling vertical variability of subsurface
641 chlorophyll maxima in a mode-water eddy. J. Mar. Res. 74: 175-199.
642 Longhurst, A. R. 2007. Ecological Geography of the Sea, 2nd Edition ed. Academic Press.
643 Lorenzen, C. J. 1966. A method for the continuous measurement of in vivo chlorophyll
644 concentration. Deep Sea Res. Oceanogr. Abstr. 13: 223-227.
645 Mackey, D. J., H. W. Higgins, M. D. Mackey, and D. Holdsworth. 1998. Algal class

abundances in the western equatorial Pacific: Estimation from HPLC measurements of chloroplast pigments using CHEMTAX. Deep-Sea Res. I 45: 1441-1468.

Martinez, J., and F. Azam. 1993. Aminopeptidase activity in marine chroococcoid cyanobacteria. Appl Environ. Microbiol. 59: 3701-3707.

Martiny, A. C., S. Kathuria, and P. M. Berube. 2009. Widespread metabolic potential for nitrite and nitrate assimilation among *Prochlorococcus* ecotypes. Proc. Natl. Acad. Sci. 106: 10787-10792.

Masuda, Y. and others 2021. Photoacclimation by phytoplankton determines the distribution of global subsurface chlorophyll maxima in the ocean. Comm. Earth Environ. 2: 128.

Mignot, A., H. Claustre, J. Uitz, A. Poteau, F. D'Ortenzio, and X. Xing. 2014. Understanding the seasonal dynamics of phytoplankton biomass and the deep chlorophyll maximum in oligotrophic environments: A Bio-Argo float investigation. Global Biogeochem. Cy. 28: 856-876.

Moore, L. R., A. F. Post, G. Rocap, and S. W. Chisholm. 2002. Utilization of different nitrogen sources by the marine cyanobacteria *Prochlorococcus* and *Synechococcus*. Limnol. Oceanogr. 47: 989-996.

Morel, A., and J.-F. Berthon. 1989. Surface pigments, algal biomass profiles, and potential production of the euphotic layer: Relationships reinvestigated in view of remote-sensing applications. Limnol. Oceanogr. 34: 1545-1562.

Ng, W. H. A., and H. Liu. 2016. Diel periodicity of grazing by heterotrophic nanoflagellates influenced by prey cell properties and intrinsic grazing rhythm. J. Plankton Res. 38: 636-651.

Paerl, H. W. 1991. Ecophysiological and trophic implications of light-stimulated amino acid utilization in marine picoplankton. Appl. Environ. Microbiol. 57: 473-479.

Rippka, R. and others 2000. *Prochlorococcus* marinus Chisholm et al. 1992 subsp. Pastoris subsp. Nov. strain PCC 9511, the first axenic chlorophyll a_2/b_2-containing

672 cyanobacterium (Oxyphotobacteria). Int. J. Syst. Evol. Microbiol. 50: 1833-1847.
673 Saijo, Y., S. Iizuka, and O. Asaoka. 1969. Chlorophyll maxima in Kuroshio and adjacent area.
674 Mar. Biol. 4: 190-196.
675 Salihoglu, B. 2009. Modeling the effect of ENSO on the lower trophic level ecosystem of the
676 Cold Tongue and the Warm Pool regions in the equatorial Pacific. J. Mar. Sys. 77: 160-
677 181.
678 Sato, M., S. Takeda, and K. Furuya. 2006. Effects of long-term sample preservation on flow
679 cytometric analysis of natural populations of pico-and nanophytoplankton. J.
680 Oceanogr. 62: 903-908.
681 Sato, M., S. Takeda, and K. Furuya. 2009. Responses of pico- and nanophytoplankton to
682 artificial iron infusions observed during the second iron enrichment experiment in the
683 western subarctic Pacific (SEEDS II). Deep Sea Res. II 56: 2745-2754.
684 Sato, M., F. Hashihama, S. Kitajima, S. Takeda, and K. Furuya. 2010. Distribution of nano-
685 sized Cyanobacteria in the western and central Pacific Ocean. Aquat. Microb. Ecol.
686 59: 273-282.
687 Sato, M., T. Shiozaki, and F. Hashihama. 2017. Distribution of mixotrophic nanoflagellates
688 along the latitudinal transect of the central North Pacific. J. Oceanogr. 73: 159-168.
689 Sato, M., and F. Hashihama. 2019. Assessment of potential phagotrophy by pico- and
690 nanophytoplankton in the North Pacific Ocean using flow cytometry. Aquat. Microb.
691 Ecol. 82: 275-288.
692 Suzuki, K., C. Minami, H. B. Liu, and T. Saino. 2002. Temporal and spatial patterns of
693 chemotaxonomic algal pigments in the subarctic Pacific and the Bering Sea during the
694 early summer of 1999. Deep-Sea Res. II 49: 5685-5704.
695 Takahashi, M., T. Nakai, T. Ishimaru, H. Hasumoto, and Y. Fujita. 1985. Distribution of the
696 subsurface chlorophyll maximum and its nutrient-light environment in and around the
697 Kuroshio off Japan. J. Oceanogr. Soc. Japan 41: 73-80.

698 Vaulot, D., W. Eikrem, M. Viprey, and H. Moreau. 2008. The diversity of small eukaryotic
699 phytoplankton (< or = 3 μm) in marine ecosystems. FEMS Microbiol. Rev. 32: 795-
700 820.
701 Veldhuis, M. J. W., and G. W. Kraay. 2004. Phytoplankton in the subtropical Atlantic Ocean:
702 Towards a better assessment of biomass and composition. Deep-Sea Res. I 51: 507-
703 530.
704 Venrick, E. L. 1999. Phytoplankton species structure in the central North Pacific 1973-1996:
705 variability and persistence. J. Plankton Res. 21: 1029-1042.
706 Xing, X., D. Zhao, L. Wang, and W. Fan. 2013. Seasonal variation characteristics of
707 subsurface chlorophyll maximum in the South Pacific subtropical gyre (in Mandarin).
708 Gaojishu Tongxin/Chinese High Technology Letters 23: 1038-1047.
709 Xiu, P., and F. Chai. 2020. Eddies affect subsurface phytoplankton and oxygen distributions
710 in the North Pacific Subtropical Gyre. Geophys. Res. Lett. 47: e2020GL087037.
711 Yasunaka, S., T. Ono, K. Sasaoka, and K. Sato. 2022. Global distribution and variability of
712 subsurface chlorophyll *a* concentrations. Ocean Sci. 18: 255-268.
713 Yue, J., M. A. Noman, and J. Sun. 2021. Kuroshio intrusion drives the *Trichodesmium*
714 assemblage and shapes the phytoplankton community during spring in the East China
715 Sea. J. Oceanol. Limnol. 39: 536-549.
716 Zettler, E. R., R. J. Olson, B. J. Binder, S. W. Chisholm, S. E. Fitzwater, and R. Michael
717 Gordon. 1996. Iron-enrichment bottle experiments in the equatorial Pacific: Responses
718 of individual phytoplankton cells. Deep Sea Res. II 43: 1017-1029.
719 Zubkov, M. V., B. M. Fuchs, G. A. Tarran, P. H. Burkill, and R. Amann. 2003. High rate of
720 uptake of organic nitrogen compounds by *Prochlorococcus* cyanobacteria as a key to
721 their dominance in oligotrophic oceanic waters. Appl. Environ. Microbiol. 69: 1299-
722 1304.
723 Zwirglmaier, K., J. L. Heywood, K. Chamberlain, E. M. Woodward, M. V. Zubkov, and D. J.

724 Scanlan. 2007. Basin-scale distribution patterns of picocyanobacterial lineages in the
725 Atlantic Ocean. Environ. Microbiol. 9: 1278-1290.
726 Zwirglmaier, K. and others 2008. Global phylogeography of marine *Synechococcus* and
727 *Prochlorococcus* reveals a distinct partitioning of lineages among oceanic biomes.
728 Environ. Microbiol. 10: 147-161.

729 **Table 1.** List of the cruises where vertical profiles of pico- and nanoplankton cell

730 concentrations were obtained. See Fig.1 for the locations of the stations.

Vessel	Cruise name	Period	Survey area
R/V Hakuho-maru	KH-03-2	Sep 2003	WN Pacific
	KH-04-3	Jul – Aug 2004	WN Pacific
	KH-08-2	Aug – Sep 2008	WN Pacific
	KH-11-10	Dec 2011 – Jan 2012	WN Pacific – ES Pacific
	KH-12-3	Jul – Aug 2012	WN Pacific
	KH-13-7	Dec 2013 – Jan 2014	South Pacific
	KH-14-3	Jun – Jul 2014	North Pacific
	KH-17-4	Aug – Sep 2017	North Pacific
	KH-18-6	Nov – Dec 2018	Eastern Indian Ocean
R/V Tansei-maru	KT-05-24	Sep – Oct 2005	East China Sea
	KT-06-21	Sep 2006	East China Sea
	KT-08-8	May 2005	Kuroshio
	KT-09-17	Sep 2009	East China Sea
	KT-10-19	Sep 2010	East China Sea
	KT-11-23	Sep 2011	East China Sea
	KT-12-24	Sep 2012	Kuroshio
R/V Shin-sei maru	KS-16-9	Jul 2016	WN Pacific
R/V Wakataka-maru	WK1006	Jun 2010	WN Pacific
	WK1705	May 2017	WN Pacific
R/V Mirai	MR10-01	Jan – Feb 2010	WN Pacific

731

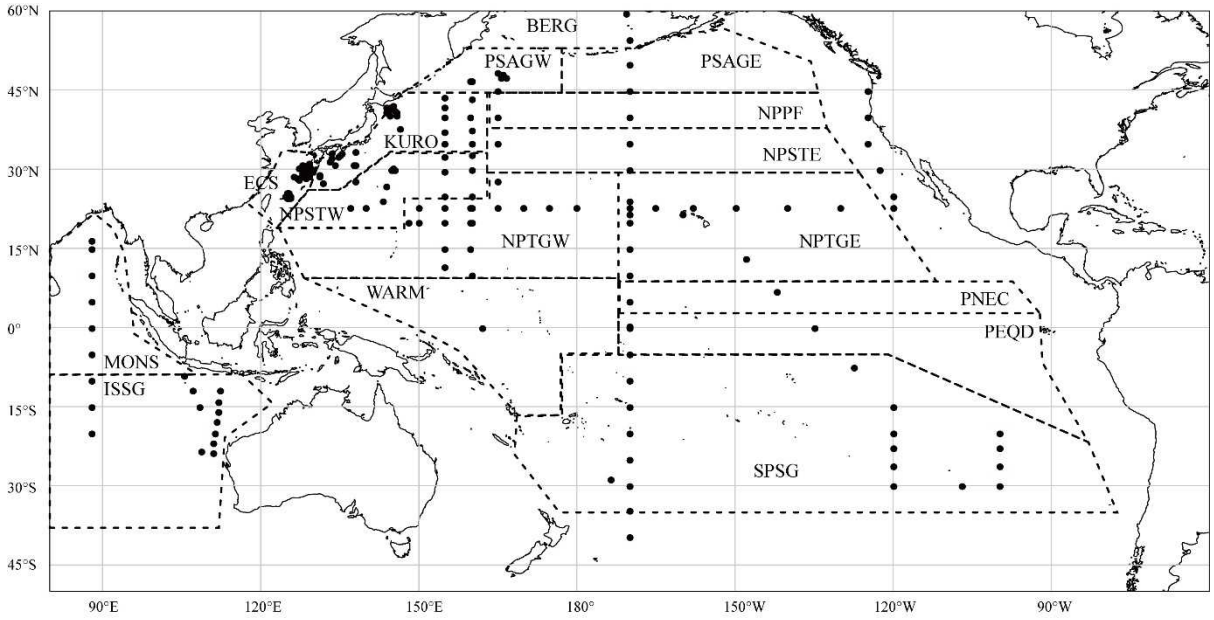

732

733 **Fig. 1.** Sampling sites. Solid circles demonstrate sampling stations. Dashed lines demonstrate

734 the borders of ocean provinces as defined by Longhurst (2007). Abbreviations: ECS: East

735 China Sea; ISSG: Indian South Subtropical Gyre; KURO: Kuroshio; MONS: Indian

736 Monsoon Gyre; NPSTW: North Pacific Subtropical Front (West); NPTGE: North Pacific

737 Tropical Gyre (East); NPTGW: North Pacific Tropical Gyre (West); PSAGW: Pacific

738 Subarctic Gyre (West); SPSG: South Pacific Subtropical Gyre.

739

740 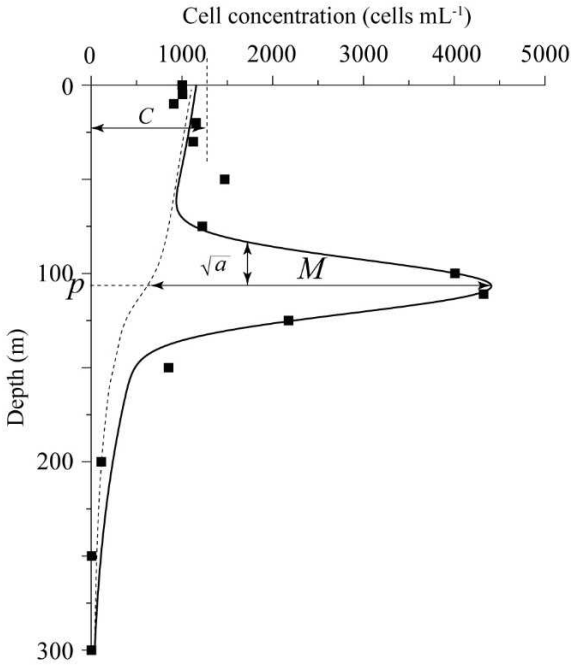

741 **Fig. 2.** Example of curve fitting to the vertical distribution of phytoplankton. The cell

742 concentration of eukaryotic pico- and nanophytoplankton was derived from St. 10 (21.5 °N,

743 165 °E) during the KH-17-4 cruise. *C*, *p*, *a*, and *M* show each parameter in Equation (1).

744 Briefly, *C* and *M* are indicative of base and peak abundance, respectively. The parameters *p*

745 and *a* indicate the depth and width of the subsurface peak, respectively.

746

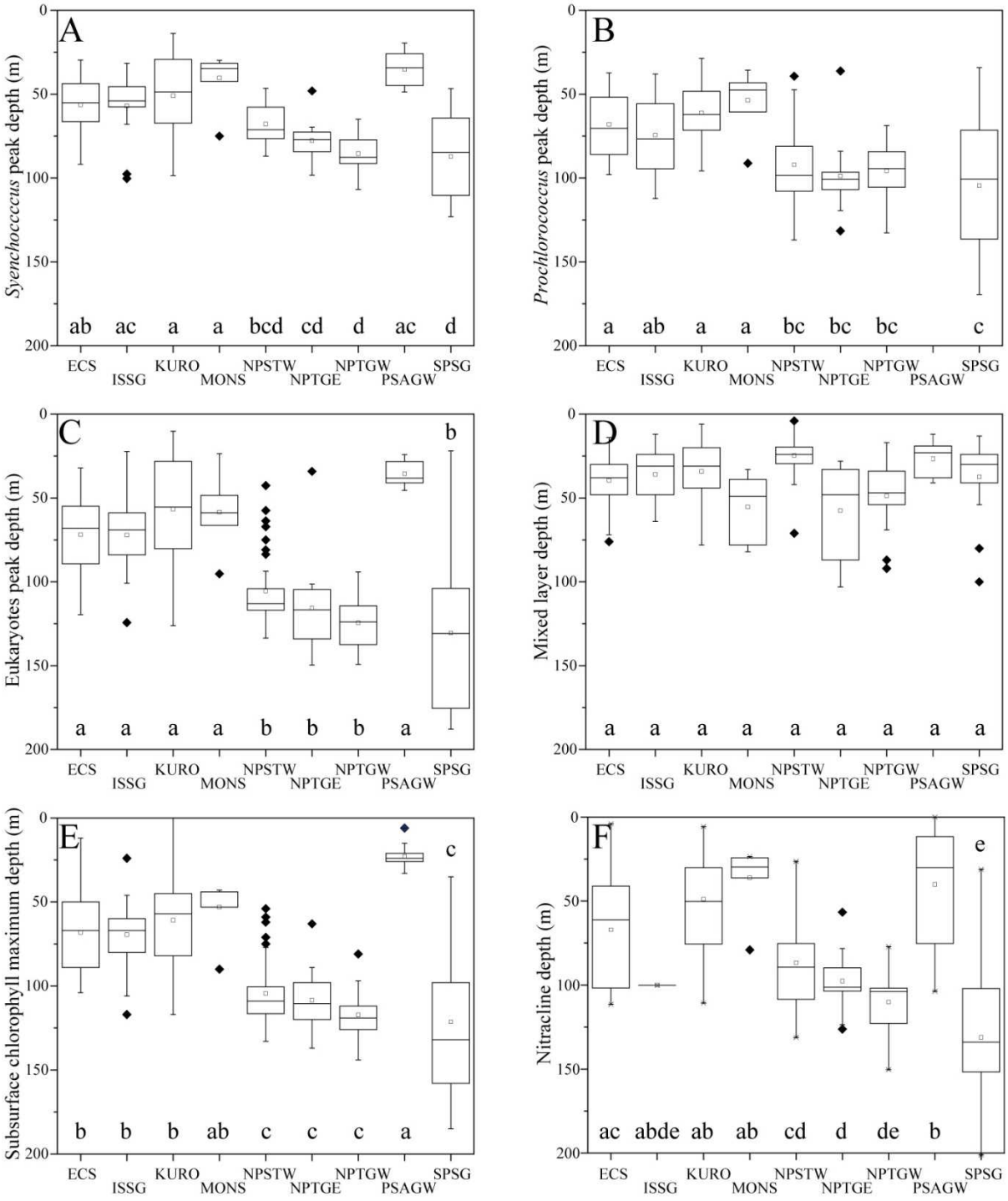

Fig. 3. Box plots of the estimated peak depths (m) of *Synechococcus* (A), *Prochlorococcus* (B), and eukaryotic phytoplankton (C), the mixed layer depth (D, m), and the SCM depth (E, m), as classified by ocean provinces (Longhurst 2007). Horizontal bars indicate the 25%,

753 50%, and 75% percentiles. Small squares and error bars demonstrate average values and
754 standard deviations. Solid diamonds demonstrate outliers. Same alphabets above or below the
755 box indicate that there was no significant difference between the two provinces (Tukey-
756 Kramer test, $p > 0.05$). Abbreviations are as in Fig. 1.
757

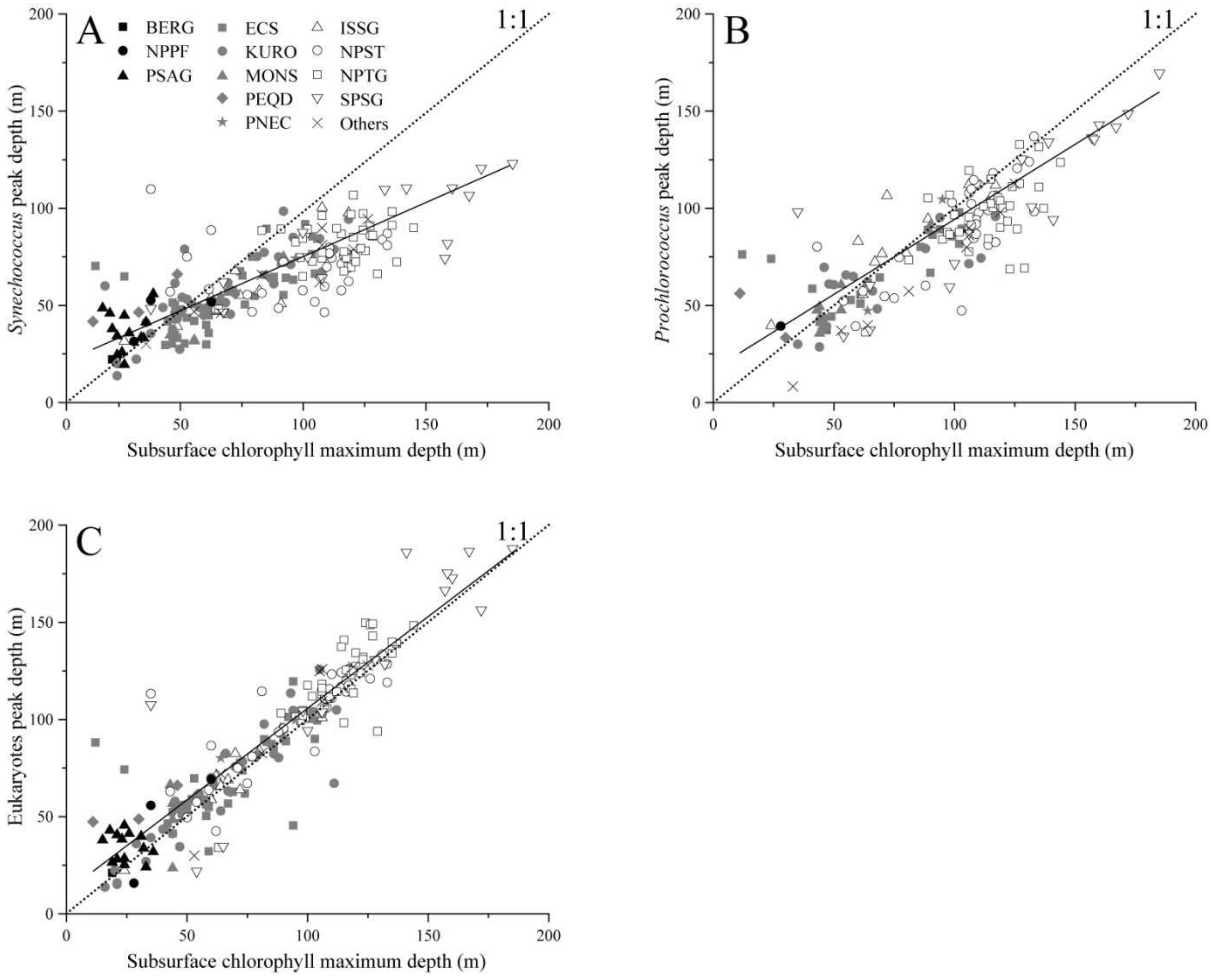

Fig. 4. Peak depths (m) of *Synechococcus* (A), *Prochlorococcus* (B), and eukaryotic phytoplankton (C) cell abundance plotted against the SCM depths (m). Different symbols indicate different ocean provinces (Longhurst 2007). Solid, gray, and blank symbols show subarctic, marginal or equatorial, and subtropical provinces, respectively. The solid line denotes a regression line. The dotted line denotes a 1:1 relationship.

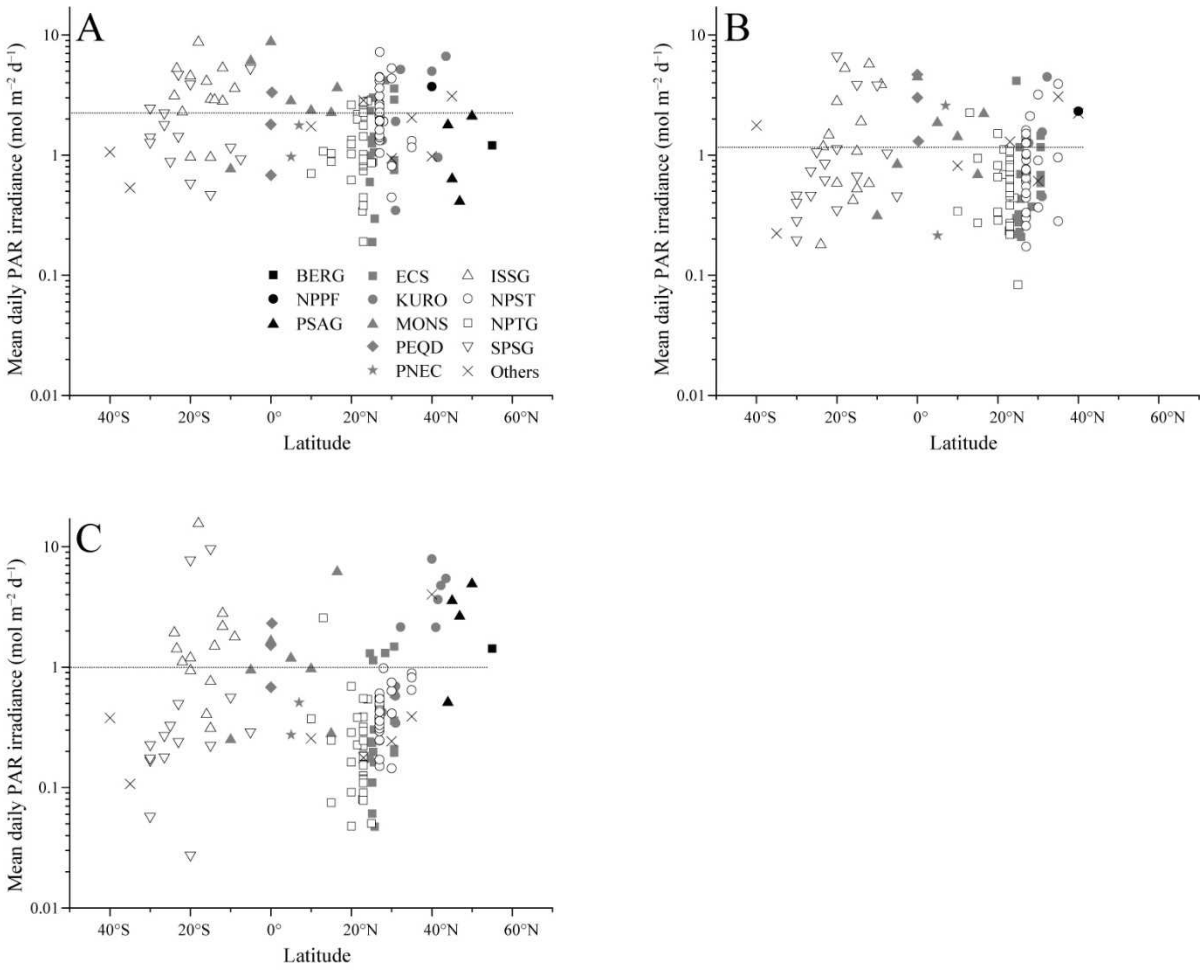

766

767 **Fig. 5.** Mean daily irradiance of photosynthetically available radiation (mol quanta m^{-2} d^{-1})

768 received by *Synechococcus* (A), *Prochlorococcus* (B), and eukaryotic phytoplankton (C) at

769 their peak depth, as plotted against latitude. Different symbols indicate different ocean

770 provinces (Longhurst 2007). Solid, gray, and blank symbols show subarctic, marginal or

771 equatorial, and subtropical provinces, respectively. Horizontal dotted lines indicate values

772 averaged over the dataset.

773

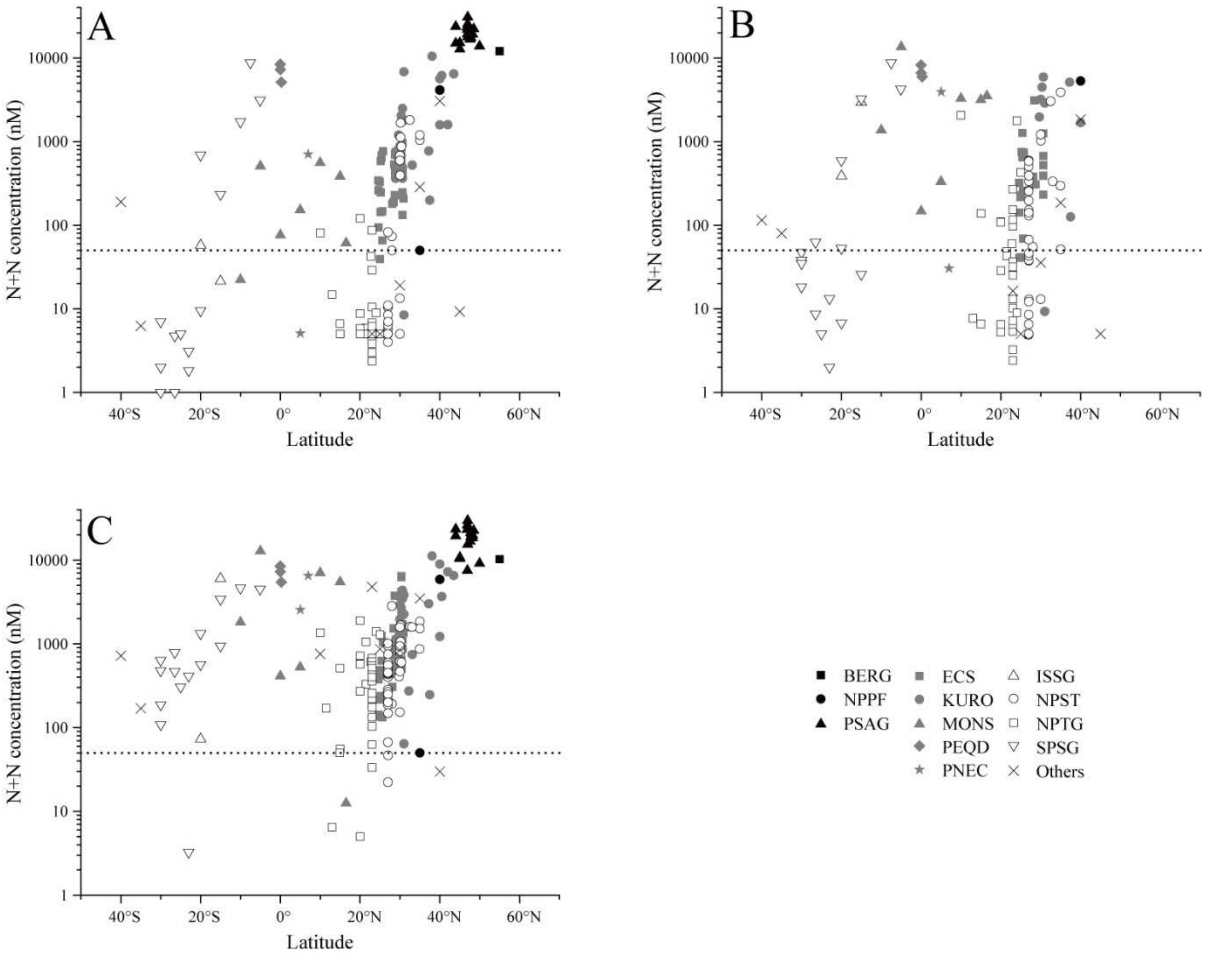

774

775 **Fig. 6.** Concentration of nitrate and nitrite (N+N) at the cell concentration peak depths of

776 *Synechococcus* (A), *Prochlorococcus* (B), and eukaryotic phytoplankton (C), as estimated by

777 linear interpolation of the discrete distribution. Different symbols indicate different ocean

778 provinces (Longhurst 2007). Solid, gray, and blank symbols show subarctic, marginal or

779 equatorial, and subtropical provinces, respectively. When the value was below the detection

780 limit of the applied method, it was plotted as the detection limit. Horizontal dotted lines

781 indicate the lower detection limit by the conventional method (0.05 μM).